V N Jayasankar[1,*],

U Vinatha[2]

J. Electrical Systems 14-2 (2018): 88-102

Regular paper

Advanced Control Approach for Shunt Active Power Filter Interfacing Wind-Solar Hybrid Renewable System to Distribution Grid

Renewable energy systems utilize the locally available energy resources and generate green energy to meet the increasing load demand. Grid integration of renewable energy systems using power electronic interfaces is the latest trend in this area of research. The non-linear loads at load centers inject current harmonics to the distribution grid at the point of common coupling and pollute the grid. The mitigation of current harmonics in the distribution grid along with the integration of renewable energy systems to the grid is the main focus of discussion in this paper. The interconnection of a hybrid solar-wind renewable energy system with the grid at the distribution level, using a voltage source inverter is presented in this paper. The inverter is controlled using the synchronous reference frame theory based control algorithm, by which the grid interfacing inverter gets additional responsibilities of shunt active power filter. Grid interfacing system consists of a 3-phase, 4-leg voltage source inverter, a dc-link capacitor and a hysteresis current controller. A self-tuning filter is designed and used in the control system for effective elimination of current harmonics. Simulation results are presented with variation in the renewable energy generation and variation in load for validating the practical application of the proposed system. All simulations are done in MATLAB-Simulink platform. The performance of 4-leg inverter in exchanging real power from renewable sources to grid along with compensating current harmonics, under balanced and unbalanced grid voltage conditions are analyzed.

Keywords: Hybrid Renewable System; Shunt Active Power Filter; Self Tuning Filter; Grid Connected Renewable; Harmonic Analysis.

Article history: Received 14 September 2017, Accepted 22 March 2018

1. Introduction

Global increase in energy demand and depleting fossil fuels resources motivate the energy engineers to find a sustainable solution. Renewable energy sources (RES) opens a wide possibility in this context. RES can be in islanded mode or grid connected mode. However, the need for energy storage devices such as battery, and the capital cost, maintenance cost and chemical pollution associated with the battery make the islanded mode less feasible for large and medium scale energy generation. The injection of the generated power directly into the main grid at the distribution level assures the maximum utilization of the locally available RES. Incorporating the grid connection of the abundantly available wind and solar energy into the grid offers a more reliable and cost-effective energy solution for the increasing energy demand. As the wind and solar energy are complimentary to each other in availability, a hybrid combination of both are preferred for a more reliable power system.

The interconnection of hybrid wind-solar RES system to the grid utilizes power electronic technology. The power electronic interfaces such as dc/dc converter and inverter assures efficient power transfer from hybrid RES to the grid [1-2]. Most commonly used wind-solar hybrid system topologies are ac shunted and dc shunted topologies. The dc

[*] Corresponding author: Jayasankar V N, Research scholar, Dept. of E&E, National Institute of Technology Karnataka Surathkal, 575025, India, E-mail: jayasankarvn@gmail.com

[1] Research scholar, Dept. of E&E National Institute of Technology Karnataka Surathkal, 575025, India

[2] Associate professor, Dept. of E&E National Institute of Technology Karnataka Surathkal, 575025, India

shunted scheme employs single inverter and it is more preferred. Moreover, the power rating of the inverter in dc shunted scheme is less than the total power rating of the two inverters used in ac shunted scheme [3-4]. In the dc shunted hybrid system, the wind and solar system require individual dc/dc converters, and they are shunted at the common dc-link of the grid interfacing inverter. By controlling the dc-link voltage of the inverter, the available real power in hybrid RES is extracted and injected into the grid. The dc-link voltage can be controlled by sensing and comparing it with the reference value, and processing the error using a PI controller [5]. The PI controller can be replaced by a fuzzy logic based dc voltage controller and has superior performance in balanced, unbalanced and distorted grid conditions according to Suresh Mikkili et.al. [6]. Ghamri A et. al. proposed the backstepping and improved backstepping controllers for dc voltage control and concluded that improved backstepping controller offers better dynamic performance than PI, but PI offers better performance in static regime [7-8].

The recent trend in the area of grid connected RES system is assigning an additional responsibility of a shunt active power filtering (SAPF) to the grid interfacing inverter. The proliferation of power electronic converters aggravated the non-linearity of load centers and deteriorated the quality of grid current at the point of common coupling (PCC) [9]. The SAPF is a common solution to improve the quality of grid current and brings the current THD within permissible limit. The use of grid interfacing system as SAPF is a cost-effective way of power quality enhancement. The inverter in SAPF acts as a current-controlled voltage source and injects compensating current to enhance the power quality of the grid current [10]. The control scheme of SAPF includes calculation of the current reference waveform for each phase of the inverter, maintenance of the dc voltage as constant, and generation of the inverter gating signals. Different methods to calculate reference current are instantaneous reactive power method, synchronous reference frame (SRF) method and peak detection method [11-12]. A comparative study between instantaneous reactive power theory, SRF theory, and peak detection method shows that under unbalance or distortions in grid voltage, SRF method is superior to others [13]. Hysteresis current control (HCC) method is widely used for generating gate pulses for the inverter control, as it is robust, simple, and has good transient response compared to other methods such as proportional integral PI controller, proportional resonant controller, repetitive controller, predictive control, deadbeat control etc. [14-16].

The recent literature on the grid integration of RES with SAPF functionality mainly focuses on the study of current harmonic elimination property by analyzing the grid current THD [17-22]. However, the details of power flow studies are not present in any literature reviewed so far. The power flow analysis is an important feasibility study to be conducted prior to the grid integration of RES systems. It ensures whether the available real power is extracted from RES system to the grid. This paper addresses the power flow analysis of the grid connected wind-solar hybrid system and validates the feasibility of the system in supplying available real power. From the literature it is also observed that the harmonic current eliminating property of SAPF can be enhanced by improving the reference current detection algorithm. The low pass filters (LPF) are widely used in detecting fundamental components of load currents in the reference current detection algorithms of SAPF. They introduce phase lags while detecting fundamental components, which adversely affects the harmonic elimination property of SAPF. The problem of additional phase lags in detecting fundamental components is addressed in this paper by introducing self-tuning filter (STF).

For a grid-connected wind-solar hybrid system with shunt active filtering functionality, an advanced controller is proposed. The controller consists of a PI controller for dc-link voltage control and the SRF theory for reference current calculation. The STF employed in the reference current algorithm introduces zero phase lags at fundamental frequency and

thereby eliminates the problems associated with phase lags. The power flow analysis is conducted on the grid-connected wind-solar hybrid system with additional SAPF functionality for a practical load profile. The input conditions are simulated based on daily wind speed and solar irradiation profiles. The grid current harmonics spectrum is analyzed to ensure that the total harmonic distortion (THD) of grid side current is maintained within the permissible IEEE standards under different grid voltage conditions.

2. System description

The overall block diagram of the system is shown in Fig. 1.The wind-solar hybrid system is connected to grid through a three phase four leg inverter at the distribution level.

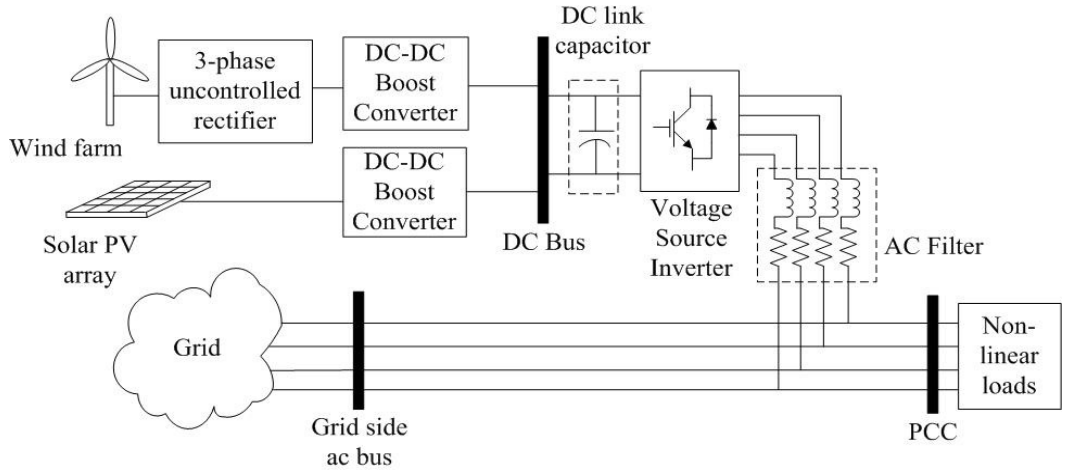

Fig. 1 Block Diagram of the Overall System

The PV system output is dc whereas wind energy system generates ac output voltage. The solar PV system output is connected to dc/dc boost converter with maximum power point tracking feature. In wind energy system the ac output is rectified using an uncontrolled rectifier and then regulated using a dc/dc boost converter [21-22]. The modeling of wind and solar energy systems are discussed in the following subsections.

2.1 Wind Energy System Modeling

The wind turbine power output can be computed as shown in Equation (1) and the aerodynamic torque is given by Equation (2) [23-24].

$$P_w = 0.5 c_p \rho A v_w^3 \tag{1}$$

$$T_w = \frac{P_w}{\omega_w} \tag{2}$$

C_P is a function of λ and β as shown in Equation (3), where λ and β are given in Equations (4) & (5) respectively. Maximum value of $C_P = 0.593$ (Betz's limit). $k_1 = 0.5$, $k_2 = 116$, $k_3 = 0.4$, $k_4 = 0$, $k_5 = 5$, $k_6 = 21$.

$$C_p(\lambda,\beta) = k_1\left(k_2 \frac{1}{\beta} - k_3 - k_4 v^x - k_5\right) e^{-k_6 \frac{1}{\beta}} + 0.0068 \tag{3}$$

$$\lambda = \frac{\omega R}{v_{wind}} \tag{4}$$

$$\frac{1}{\beta}=\frac{1}{\lambda+0.08\mathrm{v}}-\frac{0.035}{1+\mathrm{v}^3} \tag{5}$$

Mainly three types of wind energy systems are in use based on generators coupled with the wind turbine; squirrel cage induction generator (SCIG) based topology, doubly fed induction generator (DFIG) based topology, and permanent magnet synchronous generator (PMSG) based topology [23-28]. The PMSG based topology is used in this paper. The main advantage of using PMSG is that gearbox can be eliminated, and thus overall weight and cost can be reduced and improved performance and efficiency can be obtained [28].

2.2 Solar PV Modeling

Mathematical model of a photovoltaic cell is shown by Equations (6), (7), and (8) [29].

$$\mathrm{I}=\mathrm{I}_{\mathrm{solar}}-\mathrm{I}_{\mathrm{sat}}\left[\exp\left(\frac{\mathrm{V}+\mathrm{IR}_{\mathrm{s}}}{\mathrm{V}_{\mathrm{t}}\mathrm{a}}\right)-1\right]-\left(\frac{\mathrm{V}+\mathrm{IR}_{\mathrm{s}}}{\mathrm{R}_{\mathrm{p}}}\right) \tag{6}$$

$$\mathrm{I}_{\mathrm{solar}}=\left(\mathrm{I}_{\mathrm{solar,n}}+\mathrm{K}_{\mathrm{I}}\Delta\mathrm{T}\right)\left(\frac{\mathrm{G}}{\mathrm{G}_{\mathrm{nom}}}\right) \tag{7}$$

$$\mathrm{I}_{\mathrm{sat}}=\frac{\left(\mathrm{I}_{\mathrm{sc,nom}}+\mathrm{K}_{\mathrm{I}}\Delta\mathrm{T}\right)}{\exp\left(\frac{\mathrm{V}_{\mathrm{oc,nom}}+\mathrm{K}_{\mathrm{v}}\Delta\mathrm{T}}{\mathrm{aV}_{\mathrm{t}}}\right)-1} \tag{8}$$

Equation (9) represents the mathematical model of a solar array [30-31].

$$\mathrm{I}_{\mathrm{m}}=(\mathrm{N}_{\mathrm{p}}\mathrm{I}_{\mathrm{solar}})-(\mathrm{N}_{\mathrm{p}}\mathrm{I}_{\mathrm{sat}})\left[\exp\left(\frac{\mathrm{V}_{\mathrm{PV}}+(\mathrm{I}_{\mathrm{PV}}\mathrm{R}_{\mathrm{s}})(\mathrm{N}_{\mathrm{s}}/\mathrm{N}_{\mathrm{p}})}{\mathrm{N}_{\mathrm{cell}}\mathrm{V}_{\mathrm{t}}\mathrm{a}}\right)-1\right]-\left(\frac{\mathrm{V}+(\mathrm{IR}_{\mathrm{s}}(\mathrm{N}_{\mathrm{s}}/\mathrm{N}_{\mathrm{p}})}{\mathrm{R}_{\mathrm{p}}(\mathrm{N}_{\mathrm{s}}/\mathrm{N}_{\mathrm{p}})}\right) \tag{9}$$

Solar PV modules can be integrated to the grid using different topologies. From the many existing grid integration schemes, central inverter scheme is selected, as it is the most widely used technique for solar PV plants with generation capacity greater than 10 kW [32-34].

3. Control Algorithm

A shunt active filter is designed to detect the harmonic components of the load current and to inject compensating current to nullify the effect of harmonics at the point of common coupling. Fig. 2 shows the overall control schematic of the system.

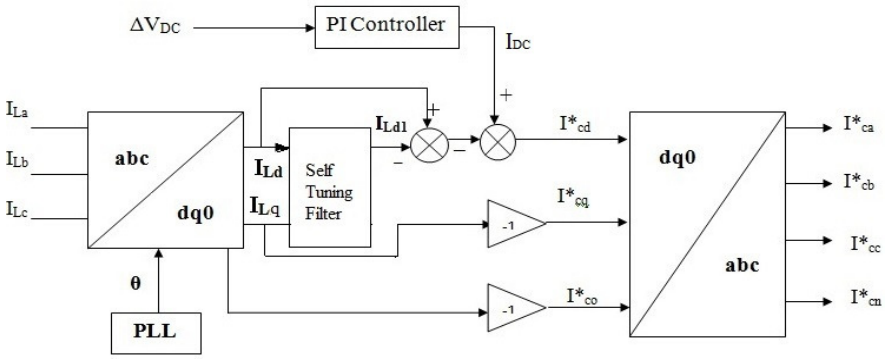

Fig. 2. Overall Control Schematic

The SAPF consists of a 4-leg voltage source inverter employed with eight IGBT switches and an energy storage capacitor. The six switches of the inverter compensate the phase currents in three phases and remaining two switches compensate the neutral current. Switching pulses are generated using fixed band HCC. SAPF consists of a reference current calculation and pulse generation system. For reference current generation, SRF method is used. In SRF control of reference current generation, the current at load center is sensed and transformed into a synchronous reference frame (dq frame) as shown in (10) & (11) [35-39]. The phase locked loop (PLL) is used for synchronizing the circuit with the grid voltage [40-42].

$$\begin{bmatrix} i_{L\alpha} \\ i_{L\beta} \end{bmatrix} = \sqrt{\frac{2}{3}} \begin{bmatrix} 1 & -1/2 & -1/2 \\ 0 & \sqrt{3}/2 & -\sqrt{3}/2 \end{bmatrix} \begin{bmatrix} i_{La} \\ i_{La} \\ i_{La} \end{bmatrix} \tag{10}$$

$$\begin{bmatrix} i_{Ld} \\ i_{Lq} \end{bmatrix} = \begin{bmatrix} \cos\omega t & \sin\omega t \\ -\sin\omega t & \cos\omega t \end{bmatrix} \begin{bmatrix} i_{L\alpha} \\ i_{L\beta} \end{bmatrix} \tag{11}$$

The current i_{Ld} is the sum of fundamental component i_{Ld1} and harmonic component i_{Ldh}. Similarly, i_{Lq} is the sum of i_{Lq1} and i_{Lqh} as shown in Equation (12).

$$\begin{bmatrix} i_{Ld} \\ i_{Lq} \end{bmatrix} = \begin{bmatrix} i_{Ld1} \\ i_{Lq1} \end{bmatrix} + \begin{bmatrix} i_{Ldh} \\ i_{Lqh} \end{bmatrix} \tag{12}$$

Fundamental components can be determined using STF. The concept of STF is introduced by Hong-scok Song [43]. The transfer function of the integrator of signals in dq frame (synchronous reference frame) is shown in Equation (13). From the frequency plot of H(s), it can be observed that it is similar to the band-pass filter. If K, a constant is introduced in H(s), Equation (13) can be modified as Equation (14).

$$H(s) = \frac{V_{xy}(s)}{U_{xy}(s)} = \frac{s + j\omega}{s^2 + \omega^2} \tag{13}$$

$$H_1(s) = \frac{V_{xy}(s)}{U_{xy}(s)} = K\frac{(s + j\omega_c) + K}{(s + K)^2 + {\omega_c}^2} \tag{14}$$

$H_1(s)$ represents a band-pass filter with no phase delay between input and output. The transfer function $H_1(s)$ represents the STF. The mathematical model of STF in dq frame is shown in Equations (15) & (16).

$$i_{Ld1}(s) = \frac{K}{s}\left(i_{Ld}(s) - i_{Ld1}(s)\right) - \frac{\omega_1}{s} i_{Lq1}(s) \tag{15}$$

$$i_{Lq1}(s) = \frac{K}{s}\left(i_{Lq}(s) - i_{Lq1}(s)\right) + \frac{\omega_1}{s} i_{Ld1}(s) \tag{16}$$

Equation (17) shows the reference currents for SAPF. The d axis reference current for harmonic elimination contain only harmonic components phase shifted by 180 degrees. An additional real power component I_{DC} is added, which is the output of DC link voltage regulator. The reference voltage and the voltage at dc link are compared and using a PI controller, the error (ΔV_{DC}) is controlled. PI controller values are set by trial and error. Equations (18) & (19) represent the inverse dq transformation for calculating three phase

equivalent of i^*_{cd} and i^*_{cq}. For neutral current compensation, reference current is taken as $i^*_{cn} = 0$.

$$\begin{bmatrix} i^*_{cd} \\ i^*_{cq} \end{bmatrix} = \begin{bmatrix} -i_{Ldh} + i_{dc} \\ -i_{Lq1} - i_{Lqh} \end{bmatrix} \tag{17}$$

$$\begin{bmatrix} i^*_{c\alpha} \\ i^*_{c\beta} \\ i^*_{c0} \end{bmatrix} = \begin{bmatrix} \cos\omega t & -\sin\omega t & 0 \\ \sin\omega t & \cos\omega t & 0 \\ 0 & 0 & 1 \end{bmatrix} \begin{bmatrix} i^*_{cd} \\ i^*_{cq} \\ i^*_{c0} \end{bmatrix} \tag{18}$$

$$\begin{bmatrix} i^*_{ca} \\ i^*_{cb} \\ i^*_{cc} \end{bmatrix} = \sqrt{\frac{2}{3}} \begin{bmatrix} 1 & 0 & \frac{1}{\sqrt{2}} \\ -\frac{1}{2} & \frac{\sqrt{3}}{2} & \frac{1}{\sqrt{2}} \\ -\frac{1}{2} & -\frac{\sqrt{3}}{2} & \frac{1}{\sqrt{2}} \end{bmatrix} \begin{bmatrix} i^*_{c\alpha} \\ i^*_{c\beta} \\ i^*_{c0} \end{bmatrix} \tag{19}$$

The 4-leg SAPF currents are sensed instantaneously and compared with the reference currents and switching pulses are generated using HCC for switching on/off the IGBT of the inverter. If the inverter current crosses the upper hysteresis limit, the switch in the upper switch in the inverter arm is turned off and lower switch is turned on. If the inverter current goes below lower hysteresis limit, the upper switch is turned on and lower switch is turned off. The controller forces the inverter current to track the reference current within the hysteresis band.

4. Results and Discussion

The real power transfer from the renewable energy system to the grid along with harmonic current filtering is done using a three-phase, 4-leg voltage source inverter. The performance of 4-leg inverter with the above-discussed control algorithm with STF has been examined under different cases. The performances of STF and LPF in detecting fundamental component of load current are compared and the results are analyzed. For analyzing the power flow, the load is varied according to an existing daily load profile data. The varying wind speed and solar irradiation are also simulated according to the daily profile for two different seasons, summer and monsoon. Simulations are done for 24 hours (1 hour = 0.5 sec in simulation) in each case. Harmonic analysis is done for, ideal grid voltage and unbalanced-undistorted grid voltage cases. Harmonic spectrum of source current is analyzed in each case for RES generation greater than load demand, and RES generation less than or equal to load demand. The simulation results presented were obtained by using MATLAB-Simulink environment. Table 1 shows the system parameters used in the simulation.

Table 1. System Parameters

Sl. No.	Particulars	Values
1	Supply Voltage	3 phase, 400 V, 50 Hz
2	Source Parameters	0.01 mH, 0.1 Ω
3	DC Link Capacitance	2350 μF
4	Voltage at DC link	600 V
5	Filter Parameters	5 mH, 0.1 Ω
6	Wind Turbine	Tower height 30 m, rotor diameter 51.2 m
7	Solar PV cell	Open circuit voltage 21.1 V, short circuit current 3.8 A

4.1 Performance comparison of LPF and STF in fundamental component detection

The performances of LPF and STF in fundamental component detection of load current are compared. Figure 3 (a) shows the magnitude and phase plots of a conventional second order low pass filter for different damping ratios (c). It can be observed from fig. 3 (a) that for all damping ratios, the low pass filter creates a phase delay at 50 Hz. Figure 3 (b) shows the magnitude and phase plots of STF for different K values. From fig. 3 (b) it can be observed that phase angle of STF is zero at 50 Hz. Also, magnitude of STF is 0 dB. As the value of K increases, the bandwidth increases. Figure 4 (a) and 4 (b) shows the load current and fundamental component of current detected using a second order LPF and STF respectively. The damping ratio of LPF is considered as 0.707 and K for STF is selected as 100. The FFT plot of phase-A grid current when LPF is used for fundamental current calculation is shown in fig. 5, and the FFT plot of phase-A grid current when STF is used for fundamental current calculation is shown in fig. 6.

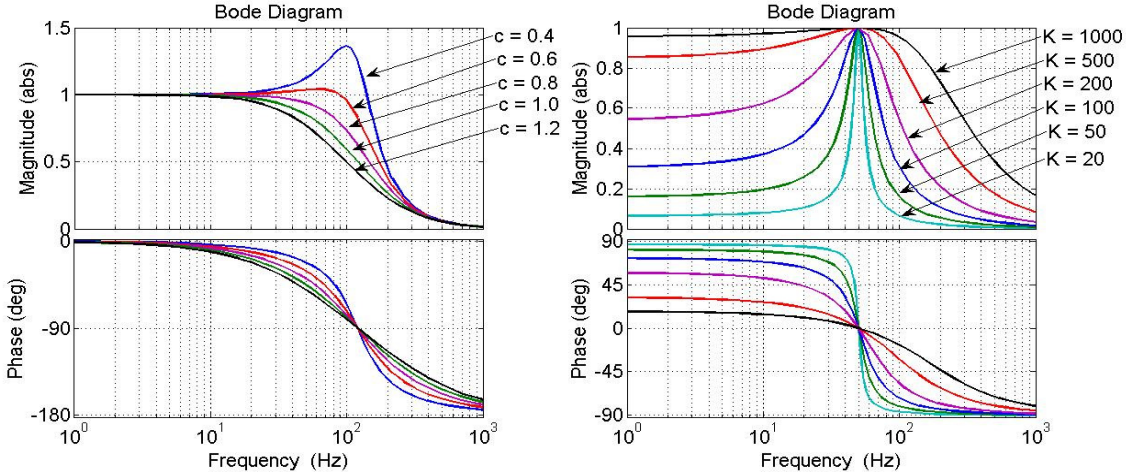

Fig. 3. Magnitude and phase plots of (a) LPF, (b) STF

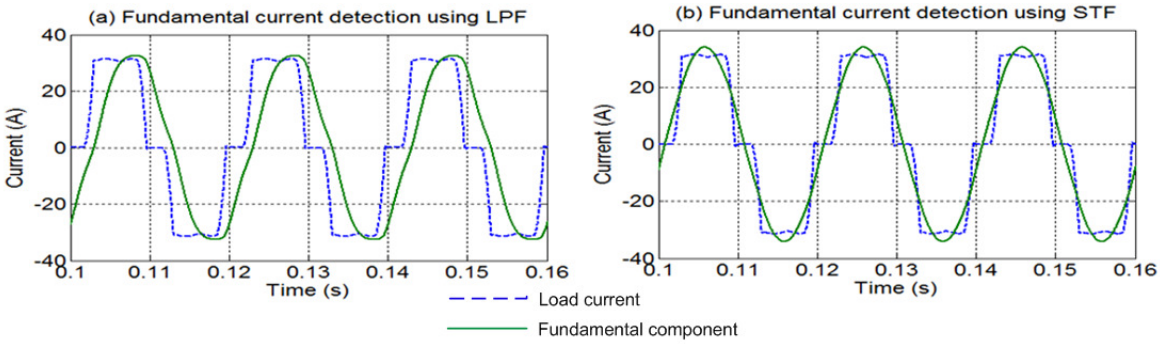

Fig. 4. Fundamental current detection (a) using LPF (b) using STF

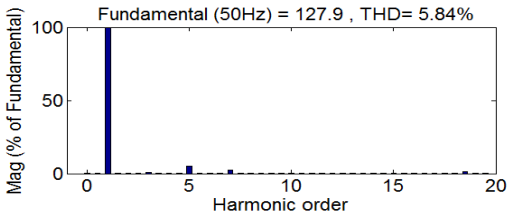

Fig. 5 FFT plot of grid current when LPF is used for fundamental component

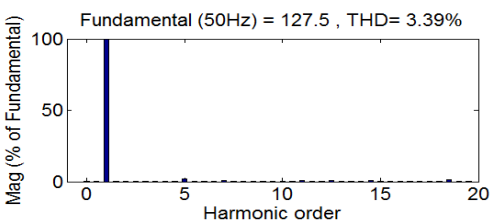

Fig. 6 FFT plot of grid current STF is used for fundamental component

It is observed from fig. 5 and fig. 6 that the grid current THD is reduced when STF is used for fundamental current calculation. The proposed control scheme is implemented with

reference current algorithm using SRF theory employed with STF and the dc link voltage controller using PI controller. The power flow analysis and harmonic analysis results are shown in the following sub sections.

4.2 Power Flow Analysis

In the grid connected wind-solar hybrid system, the generated power from the renewable sources should meet the local load demand at PCC, and excess power should be fed to the main grid [44]. Due to change in wind speed and solar radiation, the generated power varies. The load demand also varies as indicated by the load profile.

Case 1: Simulation of an average summer day

An average day of March is considered for simulation. Fig. 7 shows hourly average wind speed data for a day and Fig. 8 shows solar irradiation data for a day for the location Surathkal, India (12.9833 N, 74.7833 E) obtained from NASA website. An hourly load profile of a distribution feeder in a residential area for a day is considered for the simulation as shown in Fig. 9 (a). Load profile contains a morning peak and an evening peak. Fig. 9 (b) shows the total power generation from the wind-solar hybrid system. The power flowing from the grid to load in a day is shown in Fig. 9 (c). The voltage at the dc link is shown in Fig. 9 (d).

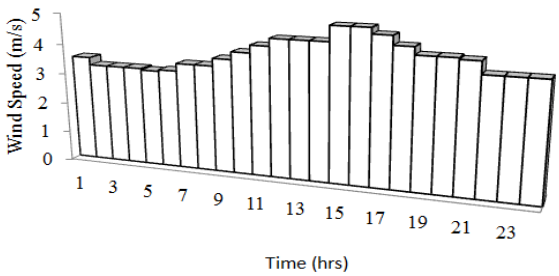

Fig. 7. Daily wind speed profile for an average summer day

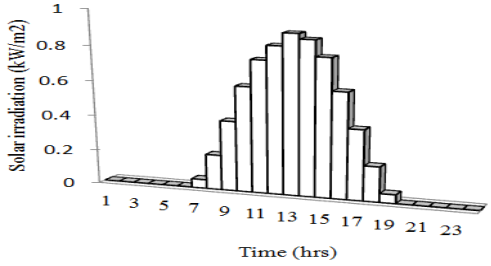

Fig. 8. Daily solar irradiation profile for an average summer day

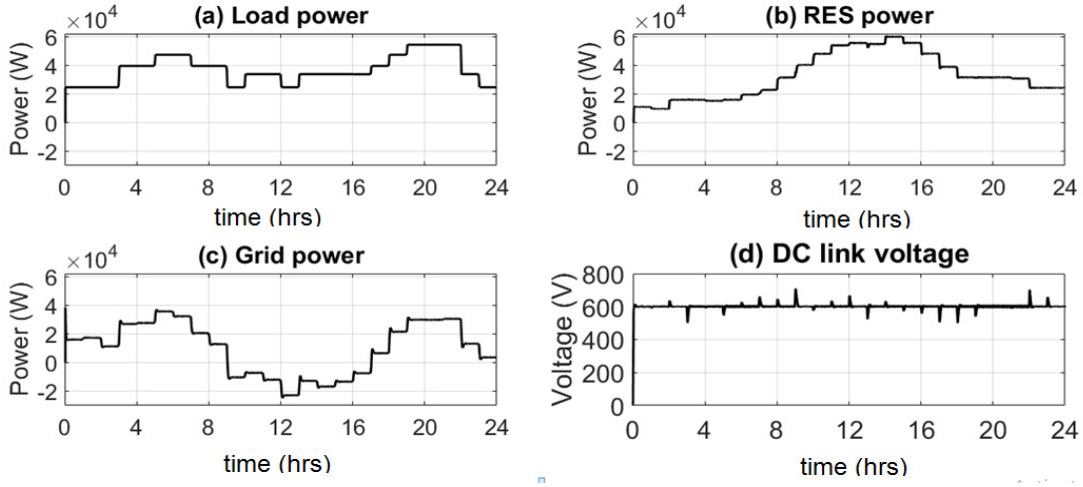

Fig. 9 (a) Daily load profile, (b) Total RES power profile for summer, (c) Grid to load power profile for summer, (d) Voltage at the dc link

From the power flow analysis for an average summer day, it is observed that the maximum power injected into the grid in a day is at 12 noon to 1 PM interval. The total generation from RES is high at noon, and at the same time load demand is low, so a part of the generated power from RES is fed to the grid. The maximum overshoot of voltage at the dc link is 11.86% and maximum steady state ripple content is 2.5%.

Case 2: Simulation of an average monsoon day

An average day of July is considered for simulation. Fig. 10 shows hourly average wind speed data for a monsoon day and Fig. 11 shows solar irradiation data for a monsoon day, for the same location mentioned above. The load profile for an average day is shown in Fig. 12 (a). Fig. 12 (b) shows the total power generation from the wind-solar hybrid system. The power flowing from the grid to load in a day is shown in Fig. 12 (c). The voltage at the dc link is shown in Fig. 12 (d).

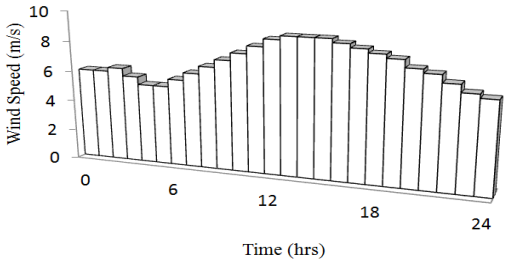

Fig. 10. Daily wind speed profile for an average monsoon day

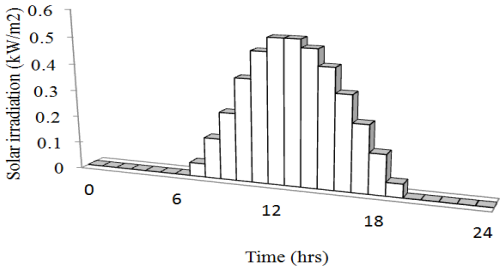

Fig. 11. Daily solar irradiation profile for an average monsoon day

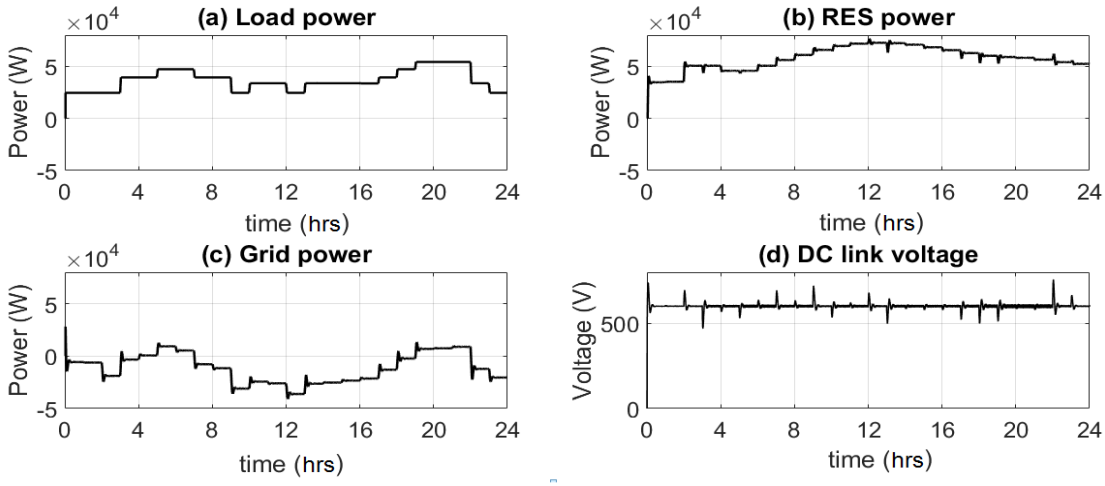

Fig. 12 (a) Daily load profile, (b) Total RES power profile for monsoon, (c) Grid to load power profile for monsoon, (d) Voltage at DC link

From the power flow analysis for an average monsoon day, it can be observed that maximum power injected into the grid in a day is at 12 noon to 1 PM interval. The total generation from RES is high at noon, and at the same time load demand is low, so a major part of the generated power from RES is fed to the grid. The maximum overshoot of voltage at the dc link is 13.66% and the maximum steady state ripple content is 2.66%. It can be concluded that the proposed controller performance is satisfactory for the given input and load conditions.

4.3 Harmonic Analysis

The grid current harmonic analysis is also done, hourly average wind speed and solar irradiation data are considered for simulation. Fig. 7 shows hourly average wind speed data for a day and Fig. 8 shows solar irradiation data for a day, for the location Surathkal, India (12.9833 N, 74.7833 E). The load profile for an average day is shown in Fig. 9 (a). Different grid conditions are considered for harmonic analysis. Harmonic spectrum of source current is analyzed in each case for RES generation greater than load demand, and RES generation less than or equal to load demand.

Case a: Balanced and undistorted grid

The three-phase balanced and undistorted grid condition is considered for simulation. Fig. 13 shows the grid voltage waveform.

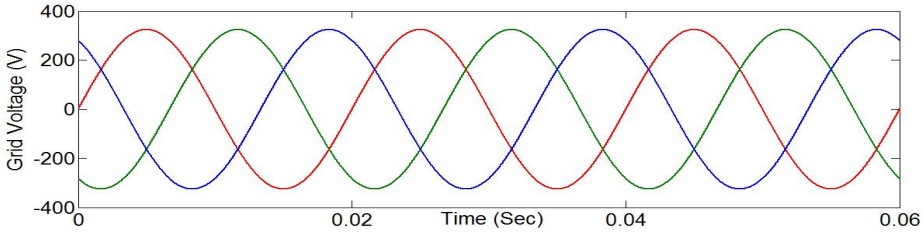

Fig. 13. Grid voltage in balanced and undistorted condition

RES generation > Load demand

The current at load center is shown in Fig. 14 (a). Fig. 14 (b), 14 (c), and 14 (d) shows compensating current, grid voltage and grid current respectively for RES generation greater than load demand condition. The grid current and grid voltage have a phase difference of 180 degrees, because power is fed to the grid at this stage.

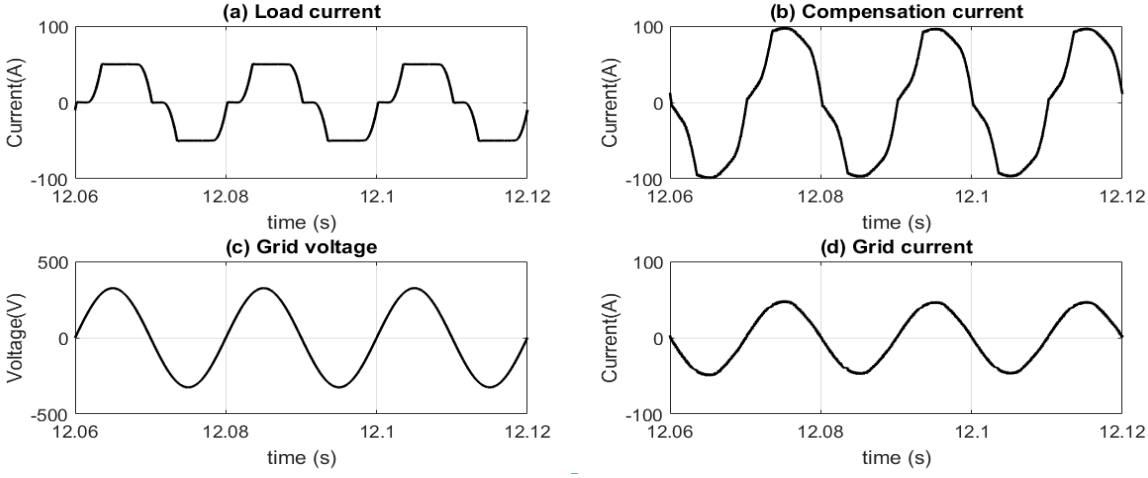

Fig. 14 (a) Current at load center, (b) Compensation current, (c) Grid voltage, (d) Grid current for RES generation > Load demand condition.

The frequency spectrum of load current and grid current for RES generation>Load demand under balanced and undistorted grid voltage condition are shown in Fig. 15 and 16 respectively.

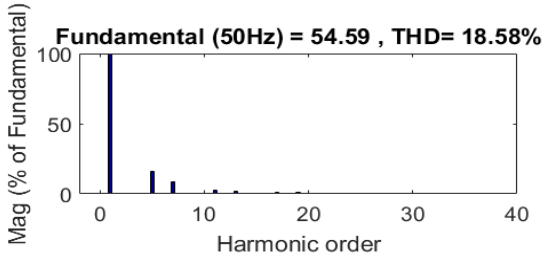

Fig. 15 FFT plot of load current for RES generation > Load demand condition

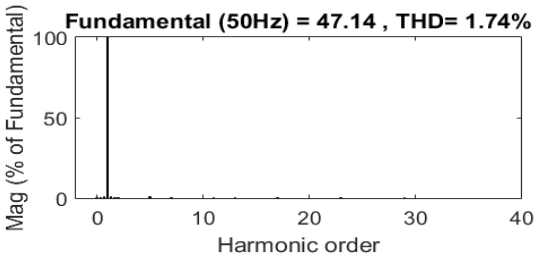

Fig. 16 FFT plot of grid current for RES generation > Load demand condition

The grid current THD is observed as 1.74%, which is well within the limits as per IEEE standards of Power Quality [45].

RES generation ≤ Load demand

The current at load center is shown in Fig. 17 (a). Fig. 17 (b), 17 (c), and 17 (d) shows compensating current, grid voltage and grid current respectively for RES generation less than or equal to load demand condition. The grid current is in phase with grid voltage, so the grid is supplying its share of power to the load. The frequency spectrum of load current and grid current for RES generation ≤ Load demand under balanced and undistorted grid voltage condition are shown in Fig. 18 and 19 respectively.

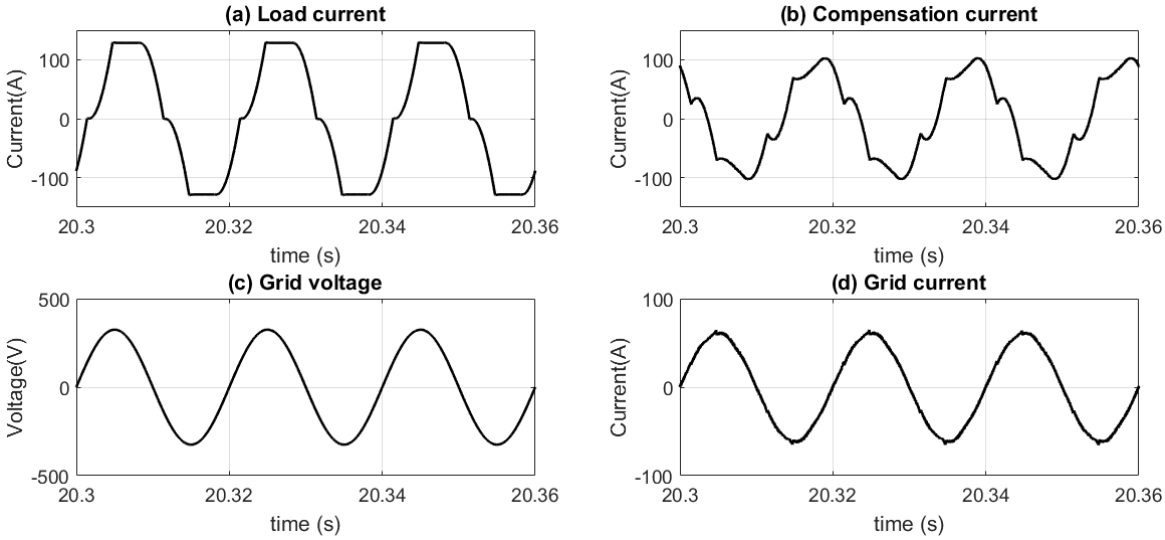

Fig. 17 (a) Current at load center, (b) Compensation current, (c) Grid voltage, (d) Grid current for RES generation ≤ Load demand condition.

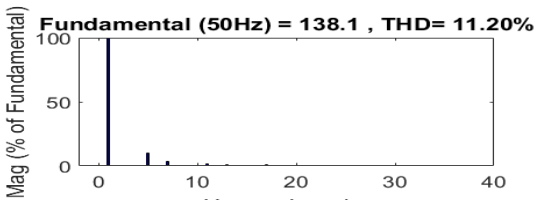

Fig. 18 FFT plot of load current for RES generation ≤ Load demand condition

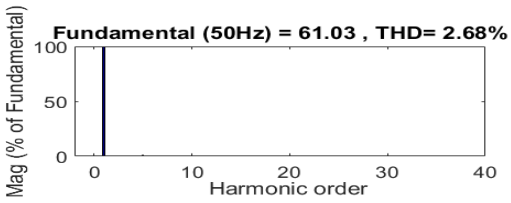

Fig. 19 FFT plot of grid current for RES generation ≤ Load demand condition

The grid current THD is observed as 2.68%, which is within the limits as per IEEE standards of Power Quality.

Case b: Unbalanced and undistorted grid

The three-phase unbalanced and undistorted grid condition is considered for simulation. Fig. 20 shows the grid voltage waveform. The maximum temporary overvoltage magnitude due to load rejection is 1.6 pu in a distribution system. The grid unbalance is simulated with a voltage magnitude of 1.6 pu in phase-A, keeping other phase voltages at nominal value.

RES generation > Load demand

The current at load center is shown in Fig. 21 (a). Figures 21 (b), 21 (c), and 21 (d) shows the compensating current, grid voltage and grid current respectively for RES generation greater than load demand condition. The grid current and grid voltage have a phase difference of 180 degrees, because power is fed to the grid at this stage. The frequency spectrum of load current and grid current for RES generation greater than load

demand under unbalanced and undistorted grid voltage condition are shown in Fig. 23 and 24 respectively

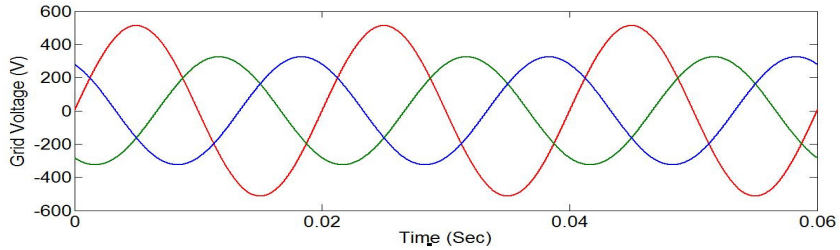

Fig. 20. Grid voltage in balanced and undistorted condition

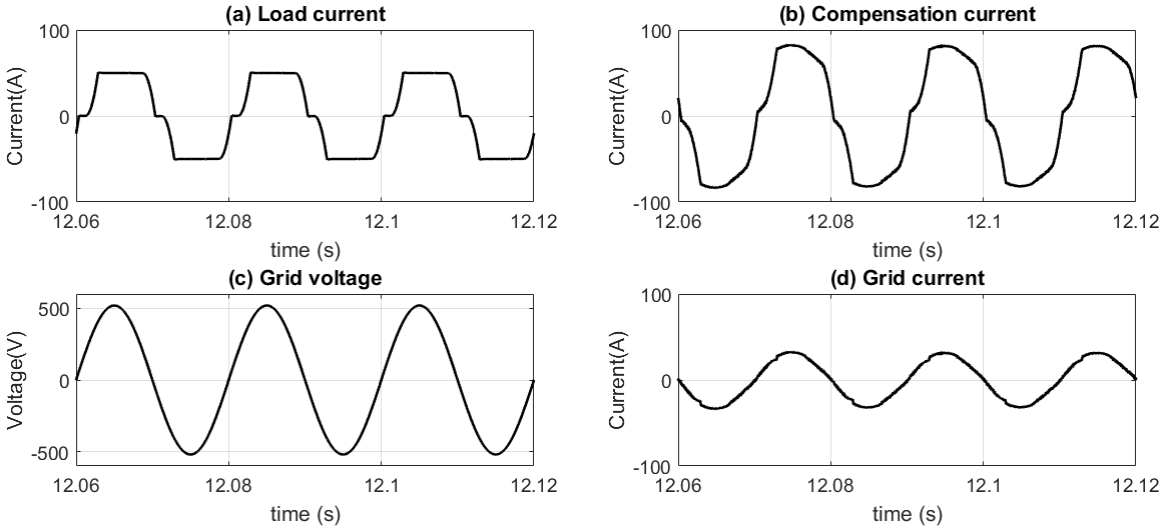

Fig. 22 (a) Current at load center, (b) Compensation current, (c) Grid voltage, (d) Grid current for RES generation > Load demand condition.

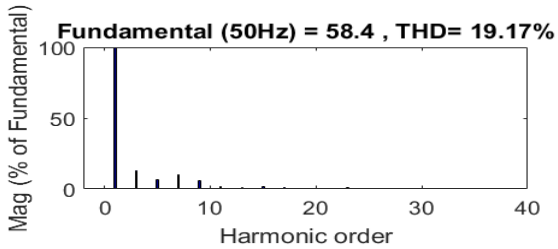

Fig. 23 FFT plot of load current for RES generation > Load demand condition

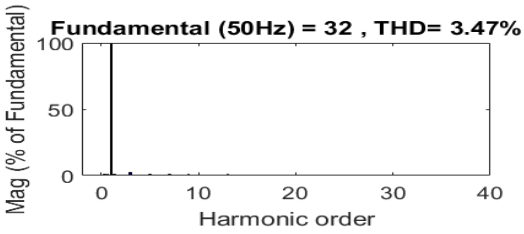

Fig. 24 FFT plot of grid current for RES generation > Load demand condition

The grid current THD is observed as 3.47%, which is well within the limits as per IEEE 519.

RES generation ≤ Load demand

The current at load center is shown in Fig. 25 (a). Figures 25 (b), 25 (c), and 25 (d) shows compensating current, grid voltage and grid current respectively for RES generation less than or equal to load demand condition. The grid current is in phase with grid voltage because grid is supplying its share of power to the load. The frequency spectrum of load current and grid current for RES generation greater than load demand under unbalanced and undistorted grid voltage condition are shown in Fig. 26 and 27 respectively.

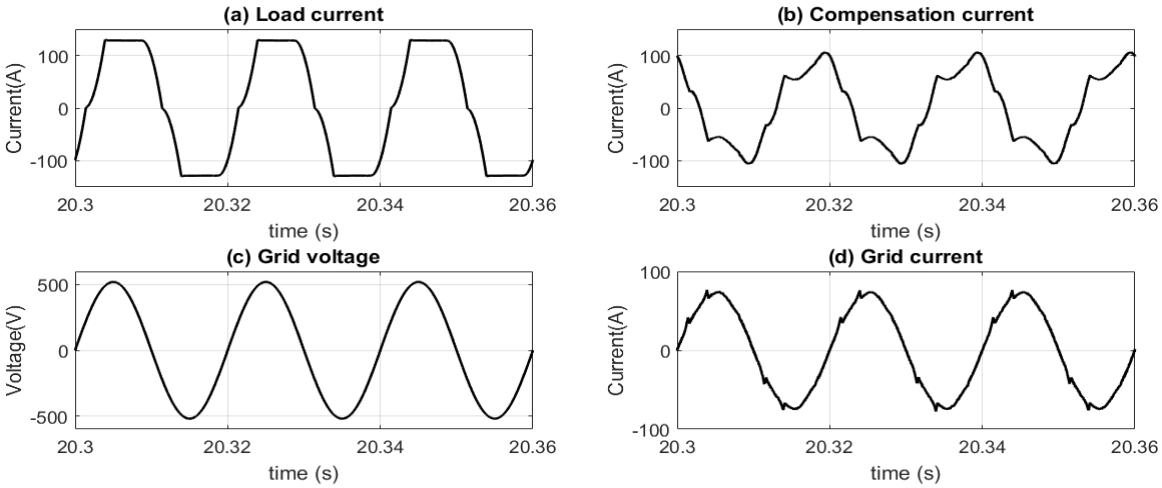

Fig. 25 (a) Current at load center, (b) Compensation current, (c) Grid voltage, (d) Grid current for RES generation ≤ Load demand condition.

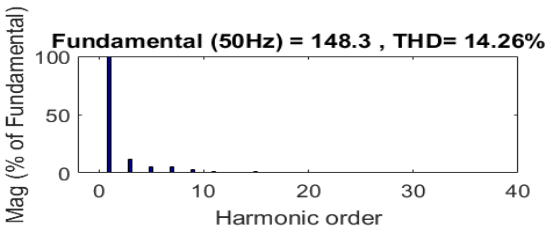

Fig. 26 FFT plot of load current for RES generation ≤ Load demand condition

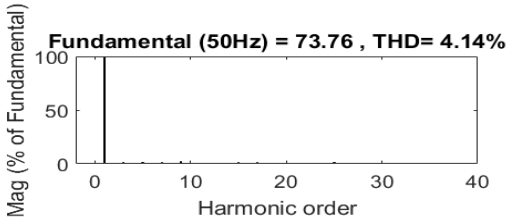

Fig. 27 FFT plot of grid current for RES generation ≤ Load demand condition

The grid current THD can be observed as 4.14%, which is within the limits as per IEEE 519.

The main contribution of this paper is the modification of reference current detection algorithm (SRF theory) using STF for more effective harmonic elimination in grid current. An improvement in the grid current THD is observed after employing STF for the detection of fundamental component of current. The authors have developed a dynamic model of a grid-connected wind-solar hybrid system with shunt active filtering functionality. The power flow analysis has been conducted in the system under varying solar irradiation, varying wind speed, and varying load conditions. The effectiveness of the dc link voltage controller in transferring available real power from the wind-solar hybrid system to the distribution grid is verified from the simulation results. The dynamic system with seasonal and daily variations in wind speed, solar irradiation and load replicate the practical conditions. The results obtained can be used for power system stability studies and generation planning for systems integrated with renewable energy sources. Harmonic analysis of grid current under different grid voltage conditions has been conducted for two different cases; RES generation greater than load demand, and RES generation less than or equal to load demand.

5. Conclusion

An advanced control algorithm employed with STF for controlling a grid connected wind-solar hybrid system with SAPF functionality is proposed. The controller allows power to flow from renewable source to load or to grid depending on the load demand and the availability of generated power in RES. It also improves the power quality at grid side. From the harmonic analysis under balanced and unbalanced grid voltage conditions it has

been observed that grid current THD is less than 5%, which is well within the limits according to IEEE 519-1992. It can be summarized that the three phase 4-leg inverter with the proposed control scheme performs satisfactorily with the following objectives, (a) The grid interconnection of the renewable energy system and (b) Current harmonics filtering.

References

[1]. S. Ravikumar and H. Vennila, Hybrid wind solar system for efficient power generation, 2017 International conference of Electronics, Communication and Aerospace Technology (ICECA), Coimbatore, India, pp. 73-79, April 2017.

[2]. M. Y. Zargar, M. U. D. Mufti and S. A. Lone, Modelling and control of wind solar hybrid system using energy storage system, 2016 International Conference on Computing, Communication and Automation (ICCCA), Noida, India, pp. 965-970, April 2016.

[3]. M. C. Yaow, S.C. Chung, and C. W. Hsu, Grid- Connected Hybrid PV/Wind Power Generation System with Improved DC Bus Voltage Regulation Strategy, Proceedings of 21st Annual Applied Power Electronics Conference and Exposition APEC06, Dallas, TX, USA, pp. 1088-1094, Mar. 2006.

[4]. G. N Hossein, A Novel Control Strategy for a Single-phase Grid-connected Power Injection System, IJE Transactions C: Aspects, Vol. 27, pp. 1841-1849, 2014.

[5]. H. Akagi, Y. Kanazawa, and A. Nabae, Instantaneous Reactive Power Compensators Comprising Switching Devices without Energy Storage Components, IEEE Transactions on Industry Applications, Vol.1, pp. 625-630, 1984.

[6]. S. Mikkili and A. K. Panda, Instantaneous Active and Reactive Power and Current Strategies for Current harmonics cancellation in 3-ph 4wire SAPF With both PI and Fuzzy Controllers, Energy and Power Engineering, Scientific Research Publishing, Vol. 3, pp. 285-298, 2011.

[7]. Ghamri, T. Mahni, M. Benchouia, K. Srairi, and A. Golea, Comparative Study between Different Controllers used in Three-phase Four-wire Shunt Active Filter, Energy Procedia, Elsevier, Vol. 74, pp. 807-816, 2015.

[8]. M. A. E. Alali and J. P. Barbot, A Lyapunov approach based higher order sliding mode controller for grid connected shunt active compensators with a LCL filter, 2017 19th European Conference on Power Electronics and Applications (EPE'17 ECCE Europe), Warsaw, pp. P.1-P.10, September 2017.

[9]. M. Suresh M, S.S. Patnaik S. S., Y. Suresh Y. and A.K. Panda, Comparison of two compensation control strategies for shunt active power filter in three phase four-wire system, Innovative Smart Grid Technologies (ISGT), 2011 IEEE PES, Hilton Anaheim, CA, USA, pp. 1– 6, January 2011.

[10]. M. Luis M., and D. Juan, Power Electronics Handbook, Butterworth-Heinemann, Boston, 2011.

[11]. H. Akagi, The state-of-the-art of active filters for power conditioning, 2005 European Conference on Power Electronics and Applications, Dresden, Germany, pp. 1-15, September 2005.

[12]. S. Bhattacharya and D. Divan, Design and implementation of a hybrid series active filter system, Power Electronics Specialists Conference, 1995. PESC '95 Record., 26th Annual IEEE, Atlanta, GA, USA,Vol.1, pp.189-195, June 1995.

[13]. V. Cardenas, L. Moran, A. Bahamondes, and J. Dixon, Comparative analysis of real time reference generation techniques for four-wire shunt active power filters, Power Electronics Specialist Conference, 2003. PESC '03. 2003 IEEE 34th Annual, Acapulco, Mexico, pp. 791-796, June 2003.

[14]. A. Hajizadeh and M. A. Golkar, Intelligent power management strategy of hybrid distributed generation system, International Journal of Electrical Power & Energy Systems, Elsevier, Vol. 29, pp. 783-795, 2007.

[15]. S. Fukuda, and T.A. Yoda, Novel current-tracking method for active filters based on a sinusoidal internal model for PWM invertors, IEEE Transactions on Industry Applications, Vol. 37, 37, pp. 888-895, 2001.

[16]. H. Mojgan, Z. A. Abu, T. Arash, S. Mohammadsoroush, An Overview on Current Control Techniques for Grid Connected Renewable Energy Systems, 2012 2nd International Conference on Power and Energy Systems (ICPES 2012), Singapore, pp. 119 – 126, November, 2012.

[17]. N. Golovanov, G. C. Lazaroiu, M. Roscia and D. Zaninelli, Power Quality Assessment in Small Scale Renewable Energy Sources Supplying Distribution Systems, Energies, Vol. 6, pp. 634 –645, 2013.

[18]. R. Belaidi, A. Haddouche, M. Fathi, M. M. Larafi and G. M. Kaci, Performance of grid-connected PV system based on SAPF for power quality improvement, 2016 International Renewable and Sustainable Energy Conference (IRSEC), Marrakech, pp. 542-545, November 2016.

[19]. M. A. Moftah, G. El-Saady and E. N. A. Ibrahim, Active power filter for power quality enhancement of photovoltaic renewable energy systems, 2016 Saudi Arabia Smart Grid (SASG), Jeddah, Saudi Arabia, pp. 1-9, December 2016.

[20]. M. Singh, V. Khadkikar, A. Chandra, Grid synchronisation with harmonics and reactive power compensation capability of a permanent magnet synchronous generator-based variable speed wind energy conversion system, IET Power Electronics, Vol. 4, pp. 122-130, 2011.

[21]. A. Beekmann, J. Marques, E. Quitmann and S. Wachtel, Wind energy converters with FACTS Capabilities for optimized integration of wind power into transmission and distribution systems, Integration of Wide - Scale Renewable Resources Into the Power Delivery System, 2009 CIGRE /IEEE PES Joint Symposium, Calgary, Alberta, Canada, pp. 1-10, July 2009.

[22]. M. Singh, V. Khadkikar, A. Chandra, Grid synchronisation with harmonics and reactive power compensation capability of a permanent magnet synchronous generator-based variable speed wind energy conversion system, IET Power Electronics, Vol. 4, pp. 122-130, 2011.
[23]. A. Beainy, C. Maatouk, N. Moubayed and F. Kaddah, Comparison of different types of generator for wind energy conversion system topologies, 3rd International Conference on Renewable Energies for Developing Countries (REDEC), Zouk Mosbeh, pp. 1-6, July 2016.
[24]. S. K. Bisoyi, R. K. Jarial and R. A. Gupta, A Review of The State Of The Art Of Generators and Power Electronics Converter Topologies for Wind Energy Conversion System, International Journal of Emerging Technology and Advanced Engineering, Vol. 3, pp. 283-291, 2013.
[25]. N.S. Patil and Y.N. Bhosle, A Review on Wind Turbine Generator Topologies, International Conference on Power Energy and Control (ICPEC), pp. 625-629, June 2013.
[26]. J. S. Sathiyanarayanan and A. Senthil Kumar, Doubly Fed Induction Generator Wind Turbines with Fuzzy Controller: A Survey, Scientific World Journal, Vol., pp. 1-8, 2014.
[27]. P. Chakrawartil, P. Jain, Complete Analysis of Doubly Fed Induction Generator Wind Turbine-Maximum Power Tracking Characteristics, International Journal of Electrical and Electronics Research, Vol. 3, pp. 12-20, 2015.
[28]. K. R. Sekhar, R. Barot, P. Patel and N. V. Kumar, A novel topology for improved DC bus utilization in PMSG based wind energy generation system, 2015 International Conference on Renewable Energy Research and Applications (ICRERA), Palermo, Italy, pp. 525-530, November 2015.
[29]. A. H. Mohammed, T. Abu, Modeling of a standalone Wind- PV Hybrid generation system using MATLAB/SIMULINK and its performance analysis, International Journal of Scientific & Engineering Research, Vol. 4, pp. 1805–1811, 2013.
[30]. E. Jamila and S. Abdelmjid, Physical Modeling of a Hybrid Wind Turbine-Solar Panel System using Simscape Language (Research note), IJE Transactions B: Applications, Vol. 27, p. 1767-1776, 2014.
[31]. R. Teodorescu, F. Blaabjerg, U. Borup and M. Liserre, A new control structure for grid-connected LCL PV inverters with zero steady-state error and selective harmonic compensation, Applied Power Electronics Conference and Exposition, 2004. APEC '04. Nineteenth Annual IEEE, Anaheim, CA, USA, pp. 580-586, September 2004.
[32]. G. V. Marcelo, E. Gazoli, and F. Ruppert, Modeling and Circuit- Based Simulation of Photovoltaic Arrays, Power Electronics Conference 2009, COBEP '09, Brazil, pp. 1244 – 1254, September 2009.
[33]. G. V. Marcelo, R. G. Jonas, and R. F. Ernesto, Comprehensive Approach to Modeling and Simulation of Photovoltaic Arrays,IEEE Transactions on Power Electronics, Vol. 24, pp.1198-1208, 2009.
[34]. D. Fei, L. Peng, H. Bibin, G. Fei, D. Chengdi and W. Chengshan, Modeling and Simulation of Gridconnected Hybrid Photovoltaic /Battery Distributed Generation System, Proceedings of International Conference on Electricity Distribution, CICED10, China, pp.1 – 10, September 2010.
[35]. S. P. Sushree and P. Anupkumar, Real time performance analysis and comparison of various control schemes for particle swarm optimization-based shunt active power filter, Journal on Electric power & Energy systems, Vol. 52, pp. 185-197, 2013.
[36]. S. Deshpande and N. R. Bhasme, A review of topologies of inverter for grid connected PV systems, 2017 Innovations in Power and Advanced Computing Technologies (i-PACT), Vellore, India, pp. 1-6, April 2017.
[37]. R. Samuel, B. Rajesh, S. Deepa and S. Jothivel, A Closed Loop Control of Quadratic Boost Converter Using PID-controller, IJE Transactions B: Applications, Vol. 27, pp.1653-1662, 2014.
[38]. S. R. Arya, B. Singh, A. Chandra and K. Al-Haddad, Power factor correction and zero voltage regulation in distribution system using DSTATCOM, 2012 IEEE International Conference on Power Electronics, Drives and Energy Systems (PEDES), Bengaluru, Karnataka, India, pp. 1-6, December 2012.
[39]. A. Zamani and H. Shahalami, Performance of a hybrid series filter in mitigating power quality problem of a grid-connected PV array interfaced with a line-commutated inverter, 2014 22nd Iranian Conference on Electrical Engineering (ICEE), Tehran, Iran, pp. 622-627, May 2014.
[40]. S. Mukhtiar, K. Vinod, Ambrish and K. V, Grid Interconnection of Renewable Energy Sources at the Distribution Level With Power-Quality Improvement Features, IEEE Transactions on Power Delivery, Vol. 26, pp. 307-315, 2011.
[41]. U. Mehmet and S. Ozdemir, 3-Phase 4-leg unified seriesparallel active filter system with ultracapacitor energy storage for unbalanced voltage sag mitigation, Electrical Power and Energy Systems, Elsevier, Vol. 49, pp. 149-159, July 2013.
[42]. T. T. Quang, A. T. Viet, P. L. Minh, Phase and Frequency Estimation for Grid-connected Inverters, Journal of Electrical Systems, Vol. 14, pp. 45-59, 2018.
[43]. S. S. Hong, Control scheme for PWM converter and phase angle estimation algorithm under voltage unbalanced and/or sag condition, Ph.D Thesis, POSTECCH university, Republic of KOREA (South), 2001.
[44]. A. Anees, Grid integration of renewable energy sources: Challenges, issues and possible solutions, 2012 IEEE 5th India International Conference on Power Electronics (IICPE), Delhi, India, pp. 1-6, December 2012.
[45]. IEEE Recommended Practices and Requirements for Harmonic Control in Electrical Power Systems, IEEE Std. 519-1992, Vol. 1, pp. 1–112, 1993.